Journal of Membrane Science 647 (2022) 120300

Contents lists available at ScienceDirect

Journal of Membrane Science

journal homepage: www.elsevier.com/locate/memsci

Ethylene and ethane transport properties of hydrogen-stable Ag^+-based facilitated transport membranes

Matthew N. Davenport, Caitlin L. Bentley, Joan F. Brennecke, Benny D. Freeman *

Department of Chemical Engineering, The University of Texas at Austin, 200 E Dean Keaton St, Austin, TX, 78712, USA

ARTICLE INFO

Keywords:
Olefin-paraffin separation
Hydrogen stability
Facilitated transport
Solid polymer electrolyte
Gas transport

ABSTRACT

A chemically specific coordination complex between solvated Ag^+ ions in polymer membranes and double-bonded olefin molecules, such as ethylene or propylene, results in a facilitated transport mechanism and increased olefin-paraffin selectivity. However, previous studies on Ag^+-containing facilitated transport membranes report poor stability of the Ag^+ carrier, especially in the presence of reducing gases, such as H_2, H_2S, and acetylene commonly present in industrial process streams. Solid polymer electrolytes consisting of crosslinked poly(ethylene glycol) diacrylate and up to 70 wt% silver bis(trifluoromethylsulfonyl)imide ($AgTf_2N$) salt are synthesized through a facile and scalable UV-crosslinking process. Following over 10 weeks of pure H_2 permeation at 4 bar and 35°C, the membrane retains 90% of its initial pure-gas ethylene-ethane selectivity. X-ray photoelectron spectroscopy shows no change in the oxidation state of the dissolved Ag^+ ions. At the highest $AgTf_2N$ concentration (70 wt%), pure-gas ethylene-ethane selectivity and permeability are 21 and 4.0 Barrer, respectively, yielding performance surpassing the polymeric gas separation membrane upper bound. High ethylene-ethane permeability selectivity results largely from increased solubility selectivity in the Ag^+-containing membranes. Dual-mode ethylene sorption is observed and modeled using a chemical equilibrium model. Diffusion coefficients are calculated according to the solution-diffusion model.

1. Introduction

Olefinic compounds are vital chemical building blocks for plastics, engineered fluids, surfactants, and plasticizers [1]. Ethylene and propylene are the largest volume organic commodity chemicals, with global production in excess of 141 million tonnes and 70 million tonnes, respectively [2]. These essential molecules are commercially produced via either steam or catalytic cracking of naphtha, ethane, or propane [3]. Steam cracking is an equilibrium process, and commercial catalytic cracking achieves approximately 30% olefin yield per pass [4–6], so purification is required to achieve polymerization grade olefin (97–99% olefin). Other emerging processes, such as oxidative coupling of methane (OCM) and methanol to olefins (MTO), in addition to the more mature Fischer-Tropsch process, also require olefin-paraffin separation [7,8]. Electrocatalytic reduction of CO_2 to ethylene does not require olefin-paraffin separation but is not currently practiced industrially due to low energy efficiency and competition with inexpensive natural gas feedstocks [9]. Because of the similar volatilities of corresponding olefin and paraffin gas pairs, the commercial separation process, cryogenic distillation, is energy and capital intensive [10,11]. Olefin splitters with hundreds of stages operate at temperatures down to −160°C and elevated pressures up to 30 bar, comprising one third of the total energy use in naphtha steam cracking [5,12]. Overall, ethylene and propylene purification account for 0.3% of global energy use [13]. These separations are essential and ubiquitous in the global chemical industry, and improvements in energy efficiency or process intensification [14] are highly desirable.

Gas separation membranes could offer energy efficiency improvements in comparison to cryogenic distillation because membranes do not require a phase change to affect separation and can be operated at ambient temperature. One immediate application of olefin-paraffin separation membranes could be recovery of the 15% of ethylene that leaves a poly(ethylene) facility as waste gas [15]. Membrane systems could also be used in conjunction with distillation as an additional pathway to improving efficiency and debottlenecking processes [16,17]. Finally, membrane-based olefin-paraffin separation could be an enabling technology for mobile, decentralized natural gas processing plants [18,19]. It has been estimated that membranes with a mixed-gas

* Corresponding author.
E-mail addresses: matt.davenport@utexas.edu (M.N. Davenport), caitlind@utexas.edu (C.L. Bentley), jfb@che.utexas.edu (J.F. Brennecke), benny.freeman@utexas.edu (B.D. Freeman).

https://doi.org/10.1016/j.memsci.2022.120300
Received 18 November 2021; Received in revised form 14 January 2022; Accepted 18 January 2022
Available online 22 January 2022

ethylene-ethane selectivity ranging from 10 to 30 could be viable for hybrid distillation processes, increasing existing capacity (debottlenecking) and potentially reducing energy intensity in the case of higher selectivity membranes [20]. However, traditional gas separation materials exhibit poor performance for olefin-paraffin separations.

Steady-state gas permeation in dense polymeric membranes occurs via solution-diffusion transport as described by Eq. (1), where the gas permeability, P_A, is the thickness- and pressure-normalized molar flux of gas A, and S_A and D_A are the solubility and diffusivity of penetrant A in the polymer matrix, respectively [21].

$$P_A = D_A S_A \tag{1}$$

Gases first dissolve in the polymer matrix at the high-pressure face of the polymer before diffusing across the membrane through transient free volume elements created through polymer thermal motion. Gas solubility is generally correlated with gas condensability, and diffusivity is inversely correlated with the size of the penetrant. The ideal selectivity between two gas species is defined as the ratio of their permeabilities, as shown in Eq. (2) [22].

$$\alpha_{AB} = \frac{P_A}{P_B} \tag{2}$$

Corresponding olefin-paraffin pairs, such as ethylene and ethane, have similar volatility (as measured by gas critical temperature or normal boiling point) and kinetic diameter, as shown in Table 1. Thus, traditional size-sieving gas separation polymers, such as polyimides, typically exhibit pure-gas selectivity values less than 5 for ethylene-ethane or 20 for propylene-propane separations [23,24]. Further, Robeson identified a fundamental tradeoff between gas permeability and selectivity across a broad range of polymeric membrane materials, so membranes exhibiting sufficient olefin-paraffin selectivity are hampered by low olefin permeability [25,26].

Facilitated transport mechanisms have been explored to improve the separation properties of polymeric membranes in several applications, such as incorporation of amine moieties to increase CO_2 transport and metal ion porphyrin complexes to increase O_2 transport [30]. Silver cations (Ag^+)—as well as other transition metal ions of similar electronic structure—coordinate reversibly with olefin compounds, but not paraffins, to form transition metal-olefin complexes, typically described by the Dewar-Chatt-Duncanson model, i.e., π backbonding [31]. Research has primarily focused on Ag^+ due to favorable electronegativity for π-complexation and low lattice energy of Ag (I) salts when compared with other transition metal salts [32]. To form an olefin facilitated transport membrane, Ag^+ is dispersed in a solvating medium, serving as a selective olefin carrier species. Olefin transport is affected by the solvent properties of the medium and the strength of interaction between Ag^+ and its corresponding anion. Various embodiments of this idea include ion exchange of Ag^+ in charged membranes [33,34], recirculated and regenerated liquid Ag^+ solutions in gas-liquid contactors [35], membranes containing ionic liquids (IL) with dissolved Ag (I) salts [36–42], and dry solid polymer electrolytes with dissolved Ag (I) salts [43–51]. Ag (I) salts are highly soluble in polymers containing ether oxygen moieties due to complexation between the ether oxygen heteroatoms and the Ag^+ cation, which is often ascribed to differences in their Lewis acidity according to Pearson's hard-soft acid base model [52,53]. Thus, polymer electrolytes formed from polyethers, such as poly (ethylene oxide) (PEO), are a convenient platform for evaluating the performance of different Ag (I) salts for olefin facilitated transport [54]. In a solid polymer electrolyte facilitated transport membrane, Ag^+ ions coordinated to the polymer backbone act as fixed-site carrier species for olefin transport [55], with olefin molecules reversibly binding to Ag^+ and transferring between sites throughout the membrane as shown in Fig. 1(a) [56–58]. Cohesive energy density is a measure of the energy necessary for free volume elements to open in a polymer matrix according to Meares' model of activated diffusion [59]. Solvated ions increase the cohesive energy density of the polymer matrix, reducing the diffusivity of all gases as depicted in Fig. 1(b) [43,59,60]. These two mechanisms together increase the selectivity of the membrane for olefins over paraffins.

Table 1
Thermophysical properties of selected corresponding olefin-paraffin pairs [27–29].

Gas	Critical Temperature [K]	Normal Boiling Point [K]	Kinetic Diameter [Å]
Ethylene	282.4	169.3	4.16
Ethane	305.4	184.6	4.44
Propylene	364.9	225.5	4.68
Propane	369.8	231.1	5.06

Ag^+ facilitated transport membranes show high olefin-paraffin selectivity [45,61]. However, the high reactivity of silver ions makes them vulnerable to poisoning by reducing gas species, such as hydrogen (H_2), hydrogen sulfide (H_2S), and acetylene [62,63]. Merkel et al. investigated a polymer electrolyte consisting of silver tetrafluoroborate ($AgBF_4$) solvated in a segmented polyether-block-polyamide copolymer (PEBAX 2533). The mixed-gas ethylene-ethane selectivity of an 80 wt% $AgBF_4$ membrane dropped from approximately 40 to unity after seven days of pure hydrogen permeation at 2 bar [64]. Industrially, H_2 concentrations of 1–4 wt% are typically found in the olefin-rich stream following dehydrogenation [65]. Though H_2S is removed prior to cracking via a Residue Desulfurization Unit (RDS), unrefined natural gas contains up to 1–2 vol% H_2S. Likewise, acetylene is hydrogenated back to ethylene, but still constitutes approximately 1% of the dehydrogenation product stream [66]. Thus, the propensity for reduction of Ag^+ to Ag^0 by reducing gases, often referred to as "carrier instability" in the literature, is one of the primary obstacles to the commercialization of facilitated transport membranes for olefin-paraffin separation [67].

To improve the stability of Ag^+ facilitated transport membranes, researchers have co-dissolved additional ionic species such as $Al(NO_3)_3$ and ionic liquids or added stabilizing agents such as peroxides and acids [68–70]. However, few studies have measured long-term stability to reducing gases. It was recently discovered that the pure-gas propylene-propane selectivity was stable with hydrogen exposure for supported ionic liquid membranes (SILMs) containing immobilized 1-hexyl-2, 3-dimethylimidazolium bis(trifluoromethanesulfonyl)imide ($hmmim^+$][Tf_2N^-]) or 1-hexyl-3-methylimidazolium bis(trifluoromethanesulfonyl)imide ([$hmim^+$] [Tf_2N^-]) ionic liquids with additional dissolved silver bis(trifluoromethanesulfonyl)imide ($AgTf_2N$) salt [38,39,71]. Our study extends this discovery to polymer electrolyte facilitated membranes by investigating the hydrogen stability and facilitated transport performance of polymeric membranes formed by direct dissolution of $AgTf_2N$ into a crosslinked poly(ethylene glycol) diacrylate (XLPEGDA) matrix.

2. Methods

2.1. Materials

$AgTf_2N$ was synthesized via an ion exchange reaction between Ag_2O (Strem Chemicals, 99%) and bistriflimic acid (HTf_2N), which was in turn obtained by reaction between lithium bistriflimide ($LiTf_2N$, Sigma-Aldrich, 99.95%) and sulfuric acid (Aldon Corp., 18 M). $LiTf_2N$ was dissolved in concentrated sulfuric acid to form a 30 wt% solution, stirred at 90°C for 3 h, and then vacuum distilled at 90°C. The product (103.2 g) was dissolved in deionized water (100 mL), and Ag_2O (85.7 g) was subsequently added (1:1 M ratio between HTf_2N and Ag_2O) before heating the mixture to 60°C and stirring for 2 h. Water was removed via a rotary evaporator, and the product was dried at 50°C under high vacuum. $AgTf_2N$ was obtained as a white solid (141.2 g, 99%) and found to be free of $LiTf_2N$ impurities using an Agilent 710-ES Inductively Coupled Plasma Optical Emission Spectrometer (ICP-OES) according to

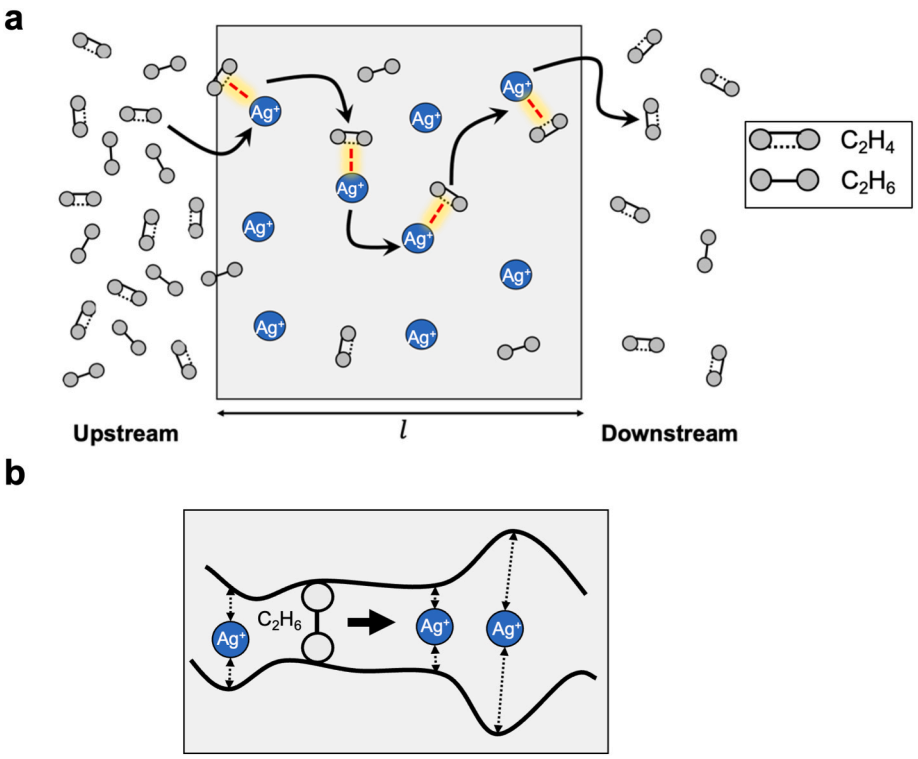

Fig. 1. Schematic illustrating: (a) Facilitated transport of ethylene between Ag^+ fixed-site carriers. (b) Interactions between Ag^+ and ether oxygen moieties serve as soft physical crosslinks, reducing gas diffusivity.

Table 2
Description of $AgTf_2N$ XLPEGDA membranes synthesized for gas permeation studies. $AgTf_2N$ concentrations correspond to final compositions of dry membranes, and EO signifies ether oxygen repeat units in the polymer.

Membrane	$AgTf_2N$ concentration [wt%]	$AgTf_2N$ concentration [mol Ag^+:mol EO]	Mass ratio of acetonitrile relative to $PEGDA_{700}$ [g:g]
XLPEGDA100	0	–	0:100
19.5 wt% $AgTf_2N$ XLPEGDA100	19.5	1:29.8	0:100
33 wt% $AgTf_2N$ XLPEGDA100	33	1:14.6	0:100
50 wt% $AgTf_2N$ XLPEGDA80	50	1:7.2	20:80
60 wt% $AgTf_2N$ XLPEGDA80	60	1:4.8	20:80
70 wt% $AgTf_2N$ XLPEGDA66	70	1:3.6	33:66

Standard Method 3120 [72] (Table S1). Acetonitrile (99.8%), 1-hydroxycyclohexyl phenyl ketone (HCPK) (99%), and poly(ethylene glycol diacrylate) of molecular weight 700 ($PEGDA_{700}$) were purchased from Sigma-Aldrich and used without further purification. The purity of HCPK was confirmed to be >99.9% via gas chromatography followed by mass spectrometry (GC-MS). The purity of PEGDA700 was confirmed to be greater than 99% via quantitative analysis of the nuclear magnetic resonance (NMR) spectra in deuterated chloroform ($CDCl_3$) recorded on a 400 MHz Agilent NMR spectrometer. GC-MS and NMR spectra are presented in Figs. S1 and S2. Ultra-high purity (99.9%) ethylene and hydrogen were purchased from Airgas, and ultra-high purity ethane was purchased from Matheson. All gases were used without further purification.

2.2. Membrane synthesis

Dense crosslinked PEGDA (XLPEGDA) membranes were synthesized via a well-known UV-crosslinking procedure [73]. Prior to crosslinking, a solution containing $AgTf_2N$, $PEGDA_{700}$, and HCPK initiator was stirred for at least 1 h. For higher concentration membranes (>33 wt% $AgTf_2N$), acetonitrile was added to the pre-polymerization solution to increase salt solubility. Details for each membrane sample are provided in Table 2. The pre-polymerization solution was sandwiched between two UV-transparent quartz plates, and crosslinking was performed in a Fischer Scientific FB UVXL-1000 crosslinking oven with 90 s of exposure to 312 nm UV light at an intensity of 3 mW cm^{-2}. Calibrated stainless steel spacers were used to control the thickness of the resulting film and ensure uniformity. Upon exposure to UV light, a free radical polymerization is initiated with reaction of the acrylate groups on either end of the difunctionalized $PEGDA_{700}$ monomer to form a three-dimensional crosslinked network [74,75]. Solvent extraction to remove any non-polymerized monomer (sol) was not performed due to the potential of also removing dissolved $AgTf_2N$. The concentration of sol following crosslinking in pure XLPEGDA films has been found to be minimal [73]. Following polymerization, the membranes were peeled from the casting plates and dried under vacuum (~1 Pa) overnight at ambient temperature, with precautions taken to limit exposure to light. Heat could not be used during the membrane drying step because the membranes showed discoloration, i.e., reduction of Ag^+, within a few hours. There was no discoloration to indicate reduction of Ag^+ due to UV exposure during crosslinking, and discoloration did not become evident until over 4 min of UV exposure as seen in Fig. S3.

2.3. Gas permeation

Films of uniform thickness were fixed to brass support disks with a filter paper backing using epoxy resin. Film thickness was measured using digital calipers (Mitutoyo, ±1 μm resolution) and ranged from 40 to 200 μm. Membranes with a thickness of 200 μm were easier to handle and developed defects less frequently than thinner samples but could also exhibit gas flux below the measurement threshold of the gas permeation apparatus at higher $AgTf_2N$ loadings. Membranes were loaded into a high-pressure Millipore filter holder, serving as the permeation cell as part of a constant-volume, variable-pressure permeation system, shown in Fig. S4 [76]. Samples were degassed overnight at 35 °C to remove any sorbed gas from the sample. The pure-gas permeabilities of H_2, ethylene, and ethane at 35 °C were measured at several transmembrane pressure points ranging between 2 and 8 bar. The rise in downstream pressure due to gas flux was measured with an MKS Baratron pressure transducer with a 1.33 kPa range, and the upstream pressure was measured with a Honeywell STJE pressure transducer with a 7 MPa range. Gas permeability is reported in units of Barrer, where 1 Barrer = 10^{-10} cm^3(STP) cm cm^{-2} s^{-1} $cmHg^{-1}$. Pure-gas ethylene and ethane permeability were measured for several samples of 50 wt% $AgTf_2N$ XLPEGDA80, and the uncertainty was estimated as two standard deviations of the mean (i.e., 95% confidence interval), as shown in Fig. S5. The relative uncertainty in permeability values for the other $AgTf_2N$ concentrations is estimated based on that of the 50 wt% $AgTf_2N$ sample.

2.4. Gas sorption

A gravimetric method was used to determine ethylene and ethane solubility in the polymer electrolyte membranes. A magnetic suspension balance manufactured by Rubotherm GmbH was used to monitor the weight change at a fixed temperature and pressure. Approximately 0.5 g of sample was added to the sample bucket and degassed to roughly 1 Pa. After any volatile impurities were evaporated, and the measured weight was constant for at least 2 h, the chamber was pressurized in incremental steps with either ethylene or ethane to a maximum pressure of 1400 kPa. Vapor-liquid equilibrium between the challenge gas and the polymer electrolyte membrane sample was considered to have been achieved once the measured weight remained constant for at least 2 h. All values were corrected for buoyancy effects according to methods reported elsewhere [77,78]. The experimental error was estimated as the average relative difference in ethylene sorption at several applied pressures between two different samples of 50 wt% $AgTf_2N$ XLPEGDA80, which was found to be 7.1%.

2.5. Density measurements

Density of the samples was measured at ambient temperature via expansion of low-pressure helium into a calibrated chamber containing the polymer sample using a Micromeritics Accupync II 1345 gas pycnometer. Measurement uncertainty is taken to be the manufacturer's estimate of ±0.002 g cm^{-3} for the instrument configuration used. Sorption of helium into the polymer sample is considered to be negligible.

2.6. Thermal analysis

The glass transition temperature (T_g) of the solid polymer electrolytes was measured via differential scanning calorimetry (DSC) using a DSC2500 manufactured by TA instruments. Samples ranging from 5 to 10 mg were measured in triplicate with three heating and two cooling steps performed for each membrane sample. Uncertainty was estimated as the 95% confidence interval calculated from the variance of the three samples. Samples were cooled to −80°C and held isothermally for 5 min before ramping to 30°C at a rate of 10 °C min^{-1}, with the reverse procedure performed for cooling steps. The T_g was measured using the half height midpoint of the step change in heat flow ascribed to the glass transition phenomena during the third heating step, as shown in Fig. S6. The accuracy of the technique was verified by comparing the T_g of the neat polymer sample (XLPEGDA100) with a value from the scientific literature [79]. Thermogravimetric analysis (TGA) was performed using a TGA/DSC 3^+ manufactured by Mettler Toledo. Samples were heated from room temperature to decomposition at a rate of 10°C min^{-1} with 50.0 mL min^{-1} N_2 flow.

2.7. Wide-angle X-ray scattering (WAXS)

WAXS spectra were collected for XLPEGDA polymer electrolytes ranging from 0 to 70 wt% $AgTf_2N$ over diffraction angles (2θ) ranging from 5° to 50° at a rate of 2° min^{-1} with a Rigaku Miniflex 600 X-ray diffractometer. The X-ray source was monochromated with a wavelength of 0.154 nm. Samples with thickness of approximately 50 μm were adhered uniformly onto a clean glass slide and spectra were collected in ambient conditions. WAXS spectra have had the background spectrum, collected on a blank glass slide, subtracted.

2.8. X-ray photoelectron spectroscopy (XPS)

XPS analyses were performed using a Kratos Axis Ultra DLD XPS, equipped with an Al Kα monochromatic X-ray source with a power set at 120 W. The photoelectrons were collected with an emission angle (EA) of 90° and from a sample area of 300 μm × 700 μm. For high-resolution spectra, the measurements were performed in constant-analyzer-energy (CAE) mode with a pass energy of 20 eV and a step size of 0.1 eV (full-width-at-half-maximum of the peak for Ag $3d_{5/2}$ is 0.77 eV). Survey spectra were collected using a pass energy of 160 eV and a step size of 1 eV. The residual pressure in the analytical chamber was ~$1x10^{-6}$ Pa. The instrument was calibrated according to ISO 15472:2001 with an accuracy of ±0.1 eV. The high-resolution spectra were processed using CasaXPS (v2.3.16, Casa Software Ltd, UK). All peaks were calibrated with respect to the adventitious hydrocarbon C 1s at 284.8 eV since a charge neutralizer was used to compensate for charge build-up. The charge neutralizer was set at 1.6 amps. Peak fitting was performed after background subtraction, which was carried out using an iterated Shirley-Sherwood algorithm [80].

2.9. Membrane stability to H_2

To evaluate the stability of the $AgTf_2N$ polymer electrolyte membranes in the presence of H_2, the pure-gas ethylene-ethane selectivity was measured following consecutive 24-hr. periods of pure H_2 permeation. Thus, pure-gas permeation experiments of ethylene, ethane, and H_2 were performed and subsequently repeated in that order. The permeability of ethylene and ethane were measured according to the method described above at a pressure of 2 bar. Two different conditions of hydrogen exposure were tested, one experiment at 2 bar and a second, more strongly reducing condition, at 4 bar. Images were taken before and after hydrogen exposure to qualitatively assess the presence of Ag^0 nanoparticles, which have been reported to form when Ag^+ is reduced to Ag^0 [81]. XPS measurements were conducted on samples following completion of the H_2 stability test and control samples from the same membrane not exposed to H_2. The binding energy peak of the $Ag3d_{5/2}$ spectra was evaluated to assess whether the average oxidation state of Ag^+ had changed. To verify the capability of the XPS technique to evaluate reduction of Ag^+ to Ag^0, membrane samples containing Ag^+ were exposed to UV light using the same conditions from the membrane synthesis procedure in order to generate Ag^0 nanoparticles. XPS was performed on a control sample not exposed to UV light, a sample exposed for 15 min, and a sample exposed for 30 min to assess progressive changes in the oxidation state of Ag^+ with additional UV light exposure.

2.10. Olefin conditioning

To evaluate the stability of membrane performance over long-term olefin permeation, a continuous pure-gas ethylene permeation experiment was performed at 3.5 bar and 35°C for 500 h in a constant-volume gas permeator as previously described. The ethylene permeability was evaluated every 12 h, with a few short interruptions in data collection due to software malfunctions. The upstream ethylene pressure was not reduced or evacuated during the experiment.

3. Results and discussion

3.1. Characterization of $AgTf_2N$ electrolyte films

The obtained polymer electrolyte films were transparent, mechanically robust, and flexible, and the apparent tackiness, which is correlated with the propensity for self-association, increased with $AgTf_2N$ concentration. Images are provided in Fig. S7. As shown in Figs. S8(a–f), thermogravimetric analysis showed a maximum of 2% mass loss prior to decomposition in the case of the 70 wt% $AgTf_2N$ XLPEGDA66 membrane, no mass loss in the case of the 50 wt% $AgTf_2N$ XLPEGDA80 membrane, and up to 1% mass loss in the case of the neat polymer and 19.5 wt% and 33 wt% $AgTf_2N$ XLPEGDA100 membranes—which contained no additional pre-polymerization solvent. The observed mass loss does not appear to correlate with the use of additional pre-polymerization solvent, so the small quantities of volatile impurities observed are attributed to a small amount of sorbed water that could not be removed by vacuum at room temperature. This finding is corroborated by a minute peak between 3000 and 3500 cm^{-1} in the FT-IR spectra of a 50 wt% $AgTf_2N$ XLPEGDA80 membrane shown in Fig. S9, which corresponds to water [82].

Wide-angle X-ray scattering (WAXS) of the polymer electrolytes showed broad peaks corresponding to an amorphous structure in contrast with the sharp, high intensity peaks of semi-crystalline linear PEO, shown in Fig. 2(a) and (b). A notable change in the diffraction pattern is evident with increasing $AgTf_2N$ concentration – the intensity of the broad $2\theta = 20^\circ$ XLPEGDA peak decreases as a peak at $2\theta = 13.5^\circ$ develops, corresponding to a larger d-spacing between regions of higher electron density. For the highest concentration, 70 wt% $AgTf_2N$, both structures seem to exist simultaneously. The structural origin of the $2\theta = 13.5^\circ$ peak is unknown, but a similar result has been observed in XLPEGDA electrolytes containing $LiTf_2N$, with a peak appearing at small diffraction angles and moderate $LiTf_2N$ concentration [83], but not at low concentration [84].

The local-scale rigidity of a polymer matrix can be characterized by the glass transition temperature, with rubbery polymers exhibiting more frequent long-range chain motion than materials below their glass transition temperature (T_g). As shown in Fig. 2(c), the T_g of the $AgTf_2N$ SPEs was measured for several $AgTf_2N$ salt concentrations, and they were rubbery at room temperature. T_g increased by 30°C relative to that of the neat polymer following incorporation of 50 wt% $AgTf_2N$, indicating reduced chain mobility and a more rigid polymer matrix, consistent with increasing cohesive energy density. Increasing the concentration of solvated Ag^+ in the membrane leads to a greater fraction of ether oxygen moieties coordinated to Ag^+ ions, which act as non-permanent physical crosslinks [85]. A maximum glass transition temperature was observed at about 50 wt% $AgTf_2N$, above which the T_g decreased. This effect has also been observed in $LiTf_2N$-containing SPE membranes with both an XLPEGDA matrix as well as linear PEO [86,87]. Once the salt concentration is above the saturation limit of the PEO chains, the matrix becomes more like a solution of saturated polymer chains in molten salt, and additional salt content has a limited effect on the T_g. The WAXS spectra of the 70 wt% $AgTf_2N$ membranes showed an additional shoulder around $2\theta = 10^\circ$ that was not observed in the 50 wt

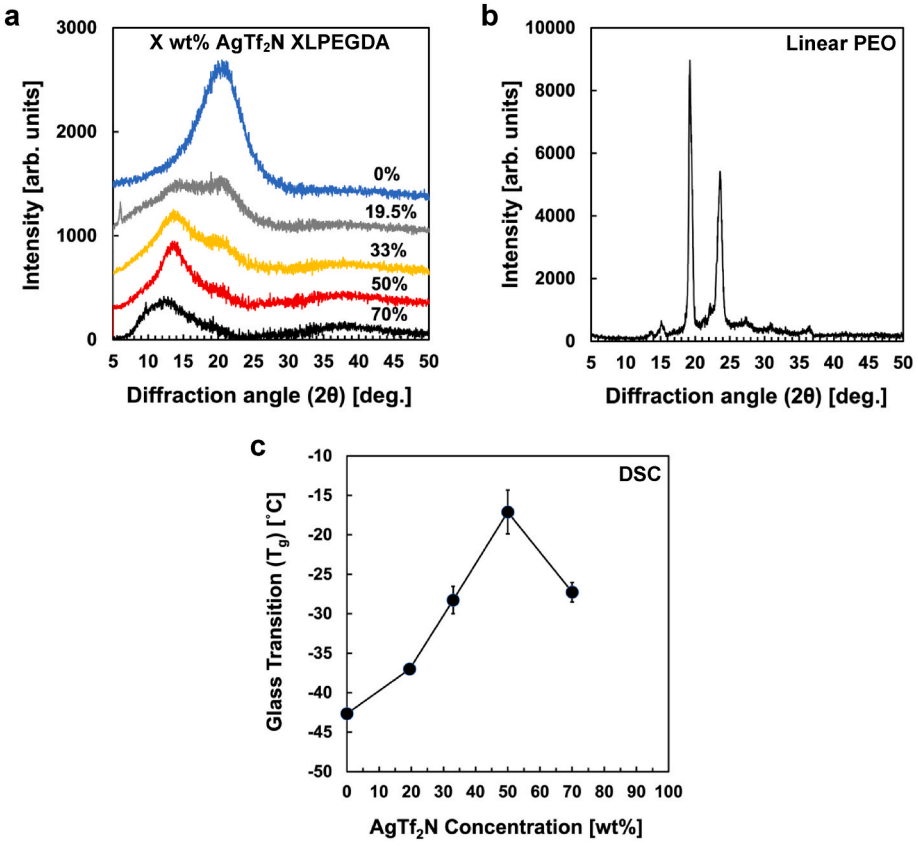

Fig. 2. Stacked WAXS spectra of (a) $AgTf_2N$-containing XLPEGDA electrolytes and (b) linear PEO with a molecular weight of 8,000,000 g mol^{-1}. (c) Glass transition temperature of XLPEGDA80 films as a function of $AgTf_2N$ concentration. Error bars are smaller than the markers for several data points.

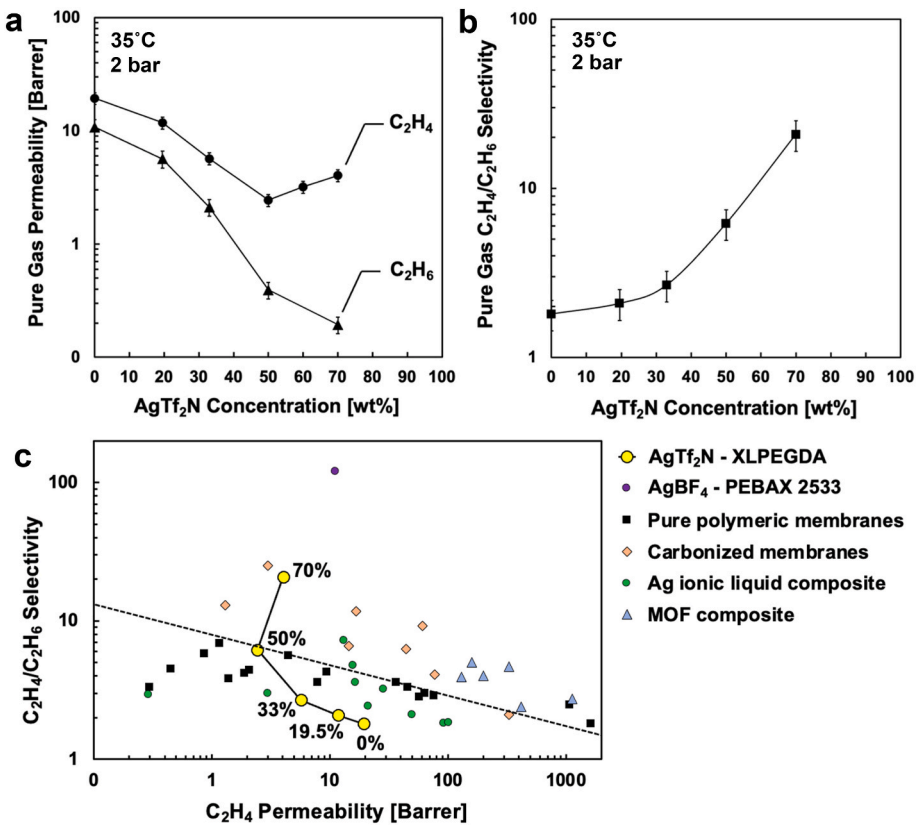

Fig. 3. Ethylene and ethane permeability (a) and selectivity (b) as a function of $AgTf_2N$ concentration in dense films of XLPEGDA80. Solid lines are provided to guide the eye. (c) Robeson plot of the pure-gas ethylene-ethane gas separation upper bound comparing the performance of $AgTf_2N$ XLPEGDA membranes with materials from the literature. Transport properties for $AgTf_2N$ SPEs were measured at 2 bar and 35°C, and the $AgTf_2N$ concentration is given in wt%. Common glassy polymeric gas separation materials are presented, along with mixed-matrix membranes containing metal organic frameworks (MOFs), carbonized membranes, $AgBF_4$-PEBAX 2533 SPE facilitated transport membranes, and Ag^+-containing ionic liquid membranes [26,45,88–94].

% $AgTf_2N$ sample, seen in Fig. 2(a), and the characteristic diffraction peaks for $AgTf_2N$ salt occurs at approximately $2\theta = 8°$ (Fig. S10).

3.2. Effect of $AgTf_2N$ concentration on gas transport

3.2.1. Permeability and selectivity

The pure-gas permeabilities of ethylene and ethane in $AgTf_2N$-XLPEGDA polymer electrolyte membranes were measured over a range of $AgTf_2N$ concentrations (Fig. 3(a)). Ethane permeability monotonically decreases with additional dissolved Ag^+, while ethylene permeability initially decreases before rising following a minimum value at 50 wt% $AgTf_2N$. Likewise, the ideal ethylene-ethane selectivity increases with $AgTf_2N$ concentration (Fig. 3(b)). The decrease in gas permeability of ethane and, initially, ethylene with $AgTf_2N$ concentration can be explained by increasing cohesive energy density, corresponding to a more rigid polymer matrix and consistent with increasing T_g (cf. Fig. 2(c)). However, at higher $AgTf_2N$ concentration, more Ag^+ sites are present to complex ethylene, and the ethylene-ethane solubility selectivity increases substantially, to be discussed in further detail. Thus, the ethylene-ethane selectivity of the membrane increases dramatically at higher $AgTf_2N$ concentrations, as seen in Fig. 3(b). Interestingly, replotting the ethylene-ethane selectivity as a function of the ratio between ether oxygen repeat units and Ag^+ yields a similar relationship to $AgBF_4$-PEBAX 2533 polymer electrolytes, shown in Fig. S11. The maximum pure-gas selectivity measured in the sample of highest concentration was 21 ± 5, with an ethylene permeability of 4.0 ± 0.5 Barrer. As shown in Fig. 3(c), this separation performance places these membrane materials above the polymeric membrane upper bound for ethylene-ethane separations.

3.2.2. Solubility

Pure-gas measurements of the ethylene and ethane solubility were undertaken. As shown in Fig. 4(a), ethylene uptake increased substantially in comparison to the neat polymer upon addition of 50 wt% $AgTf_2N$ to the crosslinked polymer matrix. Dual-mode sorption behavior was observed for ethylene in the $AgTf_2N$-containing membrane, as evidenced by the initially nonlinear relationship between the equilibrium concentration of sorbed ethylene and the applied pressure, followed by a linear trend at high pressures. The dual-mode model is comprised of two parts: preferential binding to a finite number of sites in the polymer and physical sorption described by Henry's law [95]. At low pressures, ethylene preferentially complexes with Ag^+ sites. However, these sites are saturated at higher pressures, and the isotherm becomes more linear at higher pressure, reflecting increasing contributions from Henry's law sorption. The experimental sorption and solubility of ethylene is systematically higher than the dual-mode model. This can potentially be explained by an assumption in the model that the Henry's law constant of ethylene decreases by the same factor upon the addition of 50 wt% $AgTf_2N$ as that of ethane does, a phenomenon known as "salting out". However, the specific complex between ethylene and Ag^+ may counteract the salting out effect, leading to underestimation by the model. More details on the derivation of the dual-mode model and calculation of the relevant parameters are set forth in the supporting information. Ethylene sorption in the neat polymer was linear over the pressure range considered. As shown in Fig. 4(b), neither material showed dual-mode sorption for ethane. However, ethane solubility decreased with the addition of 50 wt% $AgTf_2N$, indicating a salting-out effect where gas solubility in an electrolyte solution decreases with additional salt content [96,97]. The solubility of ethylene decreases from a maximum at infinite dilution towards a constant value at higher pressures, as seen in Fig. 4(c). This trend is consistent with expectations from a dual-mode description of the data.

Incorporation of 50 wt% $AgTf_2N$ into the XLPEGDA matrix yields a large increase in ethylene-ethane solubility selectivity (Table 3), consistent with a higher concentration of chemically specific Ag^+ binding sites. $AgBF_4$-containing electrolytes exhibit higher solubility selectivity than $AgTf_2N$-containing electrolytes due to lower lattice energy of the $AgBF_4$ salt, i.e., stronger ethylene-Ag^+ coordination enabled

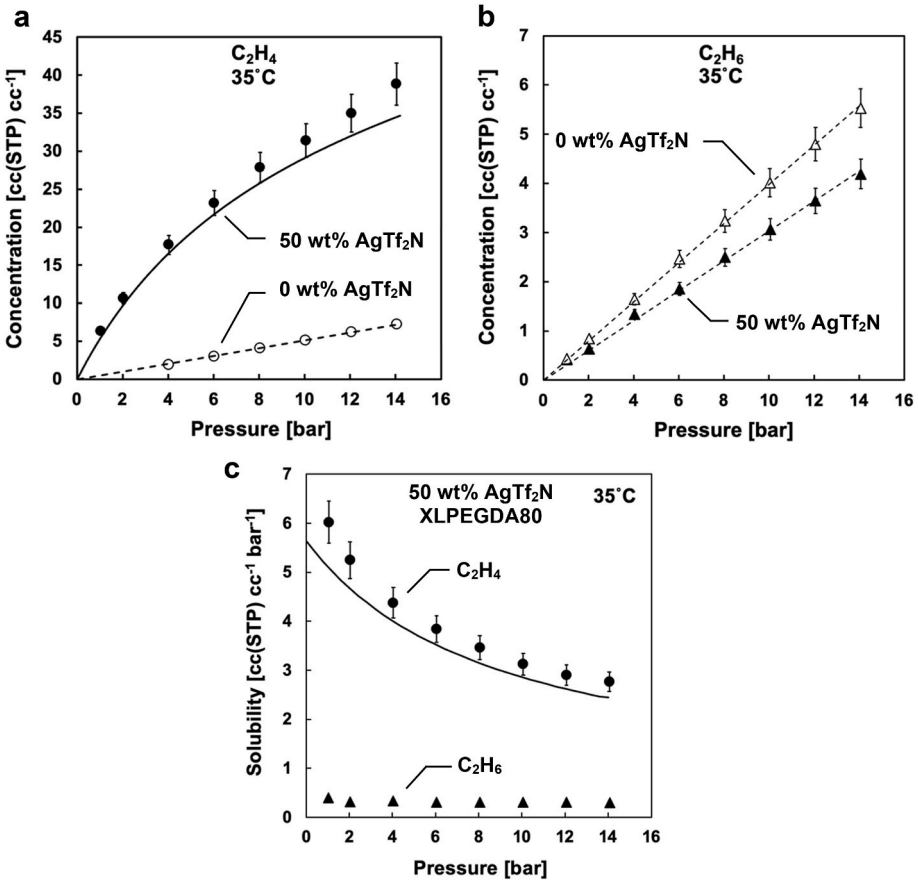

Fig. 4. Pure-gas sorption isotherms of (a) ethylene and (b) ethane in both XLPEGDA100 (i.e., 0 wt% $AgTf_2N$) and 50 wt% $AgTf_2N$ XLPEGDA80. (c) Equilibrium ethylene and ethane solubility in a 50 wt% $AgTf_2N$ XLPEGDA80 membrane as a function of gas pressure. A dual-mode sorption model (solid curves in Fig. 4(a) and (c)) is presented for ethylene sorption and solubility in the Ag-containing membrane. The rest of the data are fitted by linear regressions through the origin.

Table 3
Comparison of ethylene and ethane solubility in $AgTf_2N$-containing XLPEGDA membranes with liquids, polymers, and other polymer electrolytes [24,43,99–101].

Matrix	Type	Temperature [°C]	Pressure [bar]	$S_{C_2H_4}$ [cm^3(STP) cm^{-3} bar^{-1}]	$S_{C_2H_6}$ [cm^3(STP)cm^{-3} bar^{-1}]	$\frac{S_{C_2H_4}}{S_{C_2H_6}}$
Neat XLPEGDA100	Rubbery	35	2	0.50 ± 0.01	0.41 ± 0.01	1.2 ± 0.1
50 wt% $AgTf_2N$ – XLPEGDA80	Rubbery	35	2	5.21 ± 0.01	1.31 ± 0.01	17 ± 1
50 wt% $AgBF_4$ – PEBAX 2533	Rubbery	25	1	73	0.13	560
Poly(2,6-dimethyl phenylene oxide) (PPO)	Glassy	20	0.4	33	52	0.6
Polyimide (6FDA-6FpDA)	Glassy	35	4.2	9.8	8.1	1.2
Water	Liquid	35	8.2, 7.5	0.081	0.034	2.4
Dodecane	Liquid	25, 40	5, 3.5	2.2	3.0	0.7

by weaker ionic interactions [48,98]. However, these materials exhibit irreversible ethylene sorption and poor H_2 stability. The ethylene-ethane solubility selectivity of the Ag-containing SPE membranes is much higher than that of pure polymeric membrane materials, such as PPO and 6FDA-6FpDA, which exhibit good ethylene-ethane separation performance. Ethylene solubility is greater in 50 wt% $AgTf_2N$ XLPEGDA80

Table 4
Summary of ethylene and ethane diffusion coefficients, diffusion selectivity, and permeability selectivity in neat and $AgTf_2N$-containing XLPEGDA membranes. All values were measured or calculated at 2 bar and at 35°C. Diffusivity and diffusivity ratios calculated from independent gas permeability and sorption measurements according to the solution-diffusion model ("Sorption") agree with values obtained via the time lag analysis method ("Time lag"), shown in Fig. S13 and discussed in the supporting information.

		Sorption			Time lag		
Membrane	$\frac{P_{C_2H_4}}{P_{C_2H_6}}$	$D_{C_2H_4} \times 10^9$ [cm^2 s^{-1}]	$D_{C_2H_6} \times 10^9$ [cm^2 s^{-1}]	$\frac{D_{C_2H_4}}{D_{C_2H_6}}$	$D_{C_2H_4} \times 10^9$ [cm^2 s^{-1}]	$D_{C_2H_6} \times 10^9$ [cm^2 s^{-1}]	$\frac{D_{C_2H_4}}{D_{C_2H_6}}$
Neat XLPEGDA100	1.8 ± 0.2	300 ± 40	200 ± 30	1.5 ± 0.3	270 ± 50	180 ± 30	1.5 ± 0.4
50 wt% $AgTf_2N$ XLPEGDA80	6.3 ± 0.2	3.4 ± 0.6	9 ± 1	0.4 ± 0.1	2.4 ± 0.3	9 ± 1	0.27 ± 0.05

than liquids, such as water and dodecane, but lower than glassy polymers, such as PPO and 6FDA-6FpDA, which have non-equilibrium free volume elements.

3.2.3. Diffusivity

As shown in Table 4, diffusion coefficients for ethylene and ethane in both the neat polymer and 50 wt% $AgTf_2N$ XLPEGDA80 were calculated using independently measured pure-gas permeabilities and solubilities according to the solution-diffusion model. Ethylene and ethane diffusivities were lower in the sample containing $AgTf_2N$, consistent with a higher cohesive energy density in the salt-containing polymer and qualitatively consistent with Meares' activated diffusion model [59]. One notable trend is the reversal of the diffusivity selectivity with the addition of 50 wt% $AgTf_2N$. In the neat polymer, ethylene has a higher diffusivity than ethane because ethylene is smaller than ethane (cf. Table 1). However, the diffusion coefficient for ethane is 2.5 times larger than that of ethylene in 50 wt% $AgTf_2N$ XLPEGDA80. The selective coordination complex with Ag^+ may slow down ethylene diffusion. Reversal of ethylene-ethane diffusivity selectivity with increasing Ag^+ concentration has been demonstrated previously in Ag^+-containing polymerized ionic liquid membranes [90]. In addition, a similar phenomenon was recently reported for facilitated transport membranes containing crown ether moieties for lithium extraction applications. The diffusivity of sodium ions was slowed by complexation with the crown ether, resulting in enhanced selectivity for lithium ions which were not complexed with the crown ethers [102,103].

Eq. (2) can be re-arranged to evaluate the relative contributions of diffusivity and solubility selectivity to the overall permeability selectivity, as seen in Eq. (3).

$$\alpha_{AB} = \frac{P_A}{P_B} = \frac{D_A}{D_B}\frac{S_A}{S_B} \tag{3}$$

Thus, based on the diffusivity and solubility selectivity for ethylene-ethane separation, shown in Tables 3 and 4, the increased permeability selectivity observed in the 50 wt% $AgTf_2N$ XLPEGDA80 polymer electrolyte versus the neat polymer primarily results from increased solubility selectivity.

3.3. Ethylene plasticization

Though ethylene solubility in 50% $AgTf_2N$ XLPEGDA80 decreased with pressure (c.f. Fig. 4(c)), pure-gas ethylene permeability increased substantially with transmembrane pressure, nearly doubling after the applied pressure increased from 2 to 8 bar as shown in Fig. 5(a). Thus, as seen in Fig. 5(b), the diffusivity of ethylene also increased with transmembrane pressure, indicating plasticization of the polymer matrix by ethylene. Increasing concentration of absorbed ethylene makes the polymer matrix more rubbery, leading to higher gas permeability. Ethane permeability and diffusivity in the $AgTf_2N$ polymer electrolyte remained relatively unchanged with transmembrane pressure, which could likewise be attributed to its low solubility in the polymer matrix.

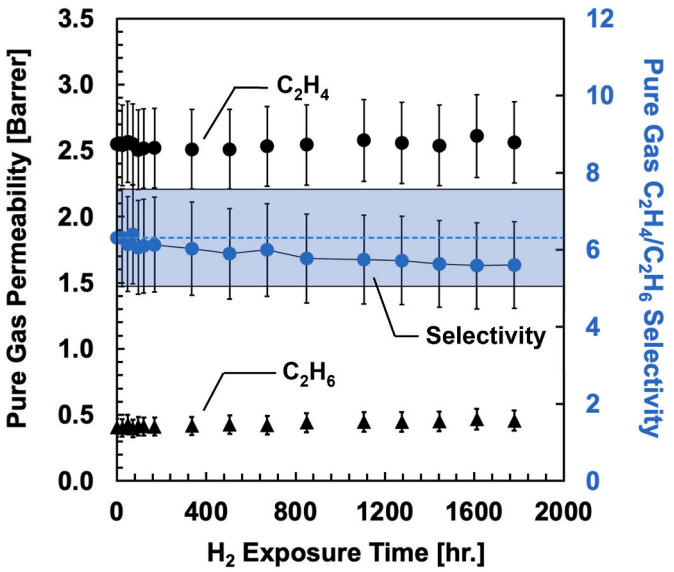

Fig. 6. Study of Ag^+ carrier stability in 50 wt% $AgTf_2N$ XLPEGDA80 membrane via long-term permeation of pure hydrogen at 4 bar and 35°C. The blue dotted line and blue band indicate the initial pure-gas C_2H_4/C_2H_6 selectivity and associated error prior to H_2 exposure. Ethylene and ethane permeability were measured at 2 bar and 35°C. The time lag of permeation was also measured during this experiment and data are presented in Fig. S14(a). (For interpretation of the references to color in this figure legend, the reader is referred to the Web version of this article.)

3.4. Membrane stability

3.4.1. Effect of hydrogen exposure on ethylene-ethane selectivity

As shown in Fig. 6, membranes containing 50 wt% $AgTf_2N$ show remarkable resistance to chemical degradation by hydrogen, which has been reported to reduce Ag^+ ions to inactive Ag^0 [62,67]. After 1779 h (over 10 weeks) of exposure to pure-gas H_2 permeation at 4 bar, which is the strongest reducing condition we are aware of in the open literature for Ag^+-containing polymeric membranes, the ethylene-ethane selectivity hardly decreased below the uncertainty of the initial value measured prior to H_2 exposure.

For comparison, as shown in Fig. 7, hydrogen stability of the

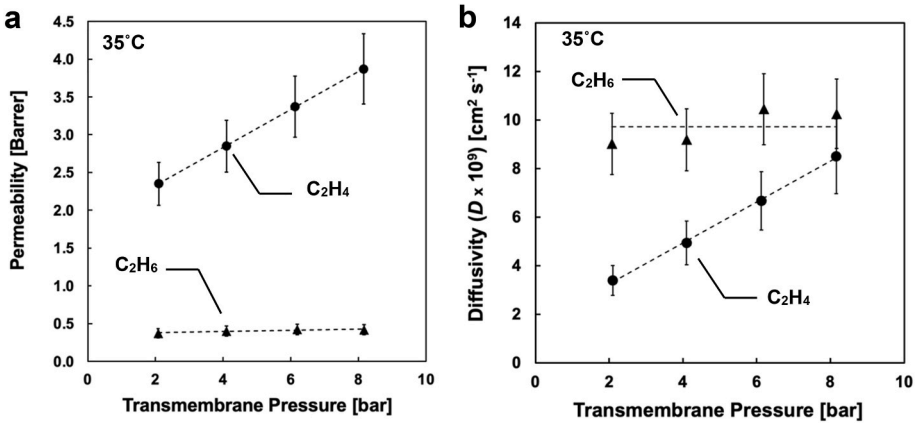

Fig. 5. (a) Pure-gas permeability of ethylene and ethane at 35°C as a function of transmembrane pressure for a 50 wt% $AgTf_2N$ XLPEGDA80 membrane sample. (b) Diffusivity calculated from the permeability values in (a) and the solubilities reported in Fig. 5(c) according to the solution-diffusion model.

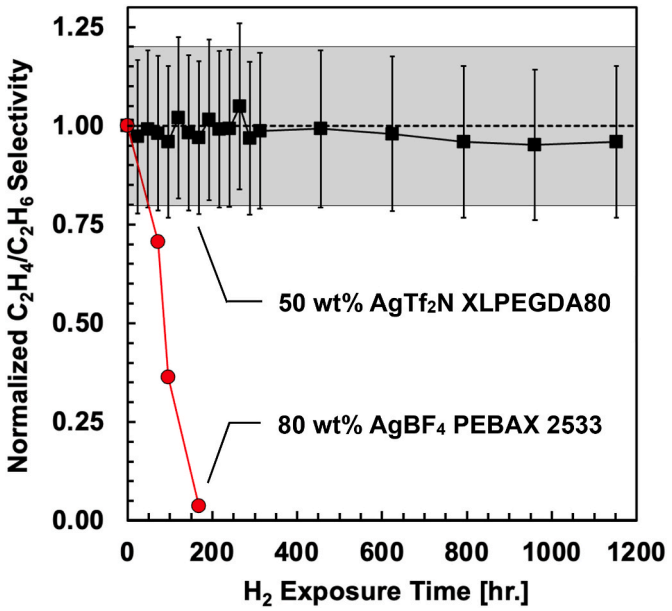

Fig. 7. Comparison of long-term ethylene-ethane selectivity stability to H_2 at 2 bar and 35°C between the $AgTf_2N$-containing membranes in this work (black squares, $\alpha_0 = 6$, pure-gas) and $AgBF_4$-containing membranes from the literature (red circles, $\alpha_0 = 40$, mixed-gas), adapted from Merkel et al. [64] The selectivity data was normalized relative to the initial selectivity value prior to hydrogen exposure. Ethylene and ethane permeability measurements were performed at 35°C and a transmembrane pressure of 2 bar. Permeability and selectivity data for this test are presented in Fig. S15. The dotted line and grey band indicate the initial normalized C_2H_4/C_2H_6 selectivity and the associated error for the 50 wt % $AgTf_2N$ XLPEGDA80 membrane prior to H_2 exposure, respectively. (For interpretation of the references to color in this figure legend, the reader is referred to the Web version of this article.)

membrane was also measured with pure-gas H_2 permeation at 2 bar, similar to the methodology of the Merkel et al. study on H_2 stability of a PEBAX 2533 membrane containing dissolved $AgBF_4$ [64]. The $AgTf_2N$-containing membranes exhibit fundamentally different behavior from that of the $AgBF_4$-containing membranes. A preparation of 80 wt% $AgBF_4$ in PEBAX 2533 loses essentially all selectivity within four days of H_2 exposure at 2 bar and 35°C, while the 50 wt% $AgTf_2N$ XLPEGDA80 sample retained 96% of its original selectivity after seven weeks.

3.4.2. *Oxidation state of Ag^+*

Upon removal of the membrane sample from the cell after H_2 permeation at 2 bar, a color change from clear to light reddish-brown was noted, as seen in Fig. 8(a). To determine whether this color change resulted from the formation of Ag^0 nanoparticles, XPS measurements were conducted to evaluate the oxidation state of Ag in the membrane. If some of the Ag^+ ions had reduced to Ag^0, then the average oxidation state should decrease. First, a control experiment was conducted to verify that XPS is sensitive to Ag^0 in the polymer electrolyte matrix. Samples of a 50 wt% $AgTf_2N$ XLPEGDA80 membrane were exposed to UV light, a strong reducing agent [104], for up to 30 min (substantially longer than the 90 s exposure used during membrane synthesis). As seen in Fig. 8(b), a significant change in color and increase in opacity was observed over time. XPS spectra of the Ag $3d_{5/2}$ orbital, shown in Fig. 8(c), confirm that the average binding energy decreased after UV exposure, moving closer to the binding energy of silver metal foil (Ag^0) and consistent with decreasing average oxidation state of silver [105].

Therefore, XPS can detect the formation of Ag^0 nanoparticles in the $AgTf_2N$ polymer electrolyte matrix. Returning to the question of Ag^+ reduction by H_2, when comparing the XPS spectra of the sample exposed to H_2 at the conclusion of the 2 bar H_2 stability test with a control sample which had been stored in a vacuum desiccator for the duration of the experiment, the binding energy remained unchanged, indicating that the average oxidation state of Ag had not been measurably changed by H_2 exposure, and thus, the majority of Ag^+ ions necessary for olefin facilitated transport had not been reduced. More investigation is needed

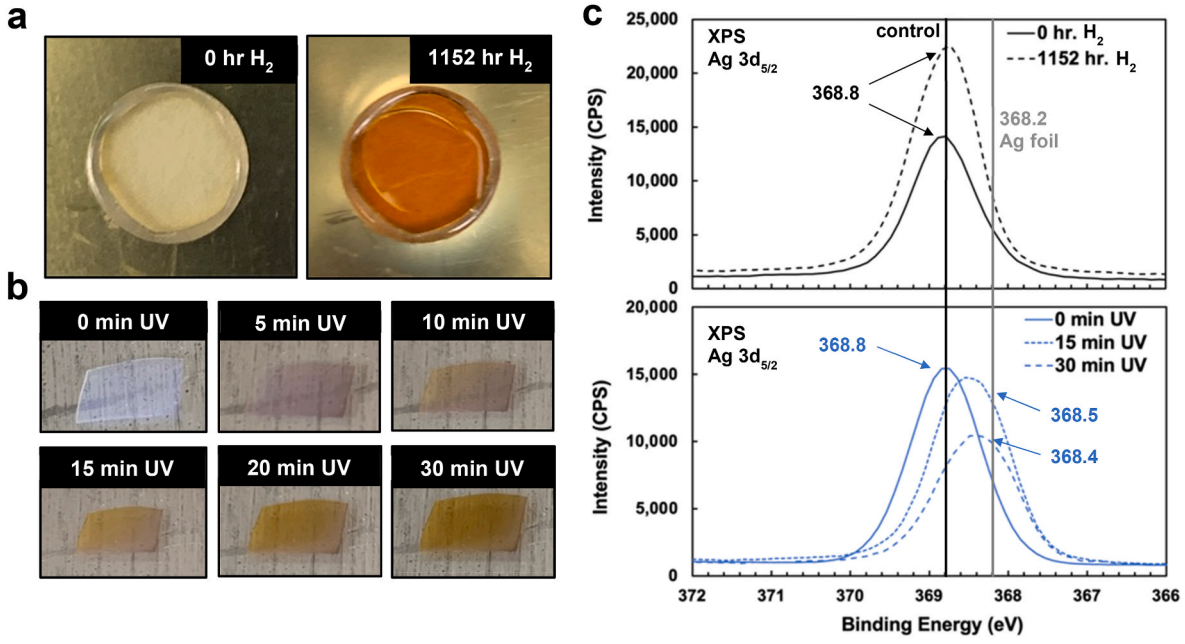

Fig. 8. (a) Color change of 50 wt% $AgTf_2N$ XLPEGDA80 membranes following 1152 h H_2 exposure (black data series in (c) and using the same membrane sample as experiment described in Figs. 6 and 7). (b) Change in color of a 50 wt% $AgTf_2N$ XLPEGDA80 membrane following exposure to UV light. (c) XPS analysis (raw data) of the oxidation state of silver in samples shown in (a) and (b). Full XPS spectra with peak fitting are presented in Fig. S16. (For interpretation of the references to color in this figure legend, the reader is referred to the Web version of this article.)

to understand the mechanism of the color change in $AgTf_2N$ XLPEGDA membranes following pure-gas ethylene, ethane, and hydrogen exposure. However, it does not appear to be a result of large-scale reduction of Ag^+ to Ag^0.

The observed H_2 stability may be a result of ionic aggregates of Tf_2N^- and Ag^+, leading to solvation shell structures which sterically hinder the formation of Ag^0 nanoparticles. Strong evidence supporting this hypothesis has been presented for $AgTf_2N$-containing ionic liquids which also exhibit H_2 stability. Studies on electrodeposition of silver metal from Ag^+ -containing ionic liquids have found that Ag^+ can be resistant to reduction when dissolved in ionic liquids. For example, cyclic voltammetry experiments on 1-ethyl-3-methylimidazolium bis(trifluoromethylsulfonyl)imide ([emim][Tf_2N]) solutions containing dissolved $AgTf_2N$ show a larger electrochemical overpotential for reduction from Ag^+ to Ag^0 versus oxidation [106–108]. The overpotential is a cumulative effect of various resistances, including kinetic, and measures the amount of energy needed to initiate a electrochemical reaction beyond the ideal case. So, a larger overpotential for reduction as compared to oxidation could indicate an additional electrochemical energy barrier not present during oxidation, i.e., a steric effect inhibiting nanoparticle nucleation. Tf_2N^- is a relatively large, weakly-coordinating anion, and forthcoming studies indicate that ionic aggregates of Ag^+ and Tf_2N^- in the ionic liquid solution leads to this steric effect, thereby promoting H_2 stability [39]. Based on the distance between Ag^+ ions, this steric effect may well be present in the $AgTf_2N$ XLPEGDA membranes. A crude geometric estimation of the interparticle distance, assuming that Ag^+ ions are evenly distributed throughout the membrane, is given by Eq. (4), where r is the interparticle distance and C is the molar concentration of Ag^+ [109].

$$r = (C)^{-\frac{1}{3}} \tag{4}$$

The interparticle distance between Ag^+ for a XLPEGDA80 membrane containing 50 wt% $AgTf_2N$ is 9.3 Å, as shown in Table 5. The ionic radius of Ag^+ is about 1.2 Å, and the width of Tf_2N^- anions (in the orientation where the amide group is coordinated to Ag^+) has been separately calculated to be 5.1 Å or 6.6 Å [110–112]. Thus, the distance between Ag^+ cations is similar in size to coordinated Tf_2N^- anions which may be present as a solvation shell structure where multiple Tf_2N^- coordinate to a single metal cation [113], potentially causing steric inhibition of Ag^0 nanoparticle nucleation.

3.4.3. *Effect of long-term H_2 permeation on solubility and diffusivity*

The permeation time lag was evaluated for each measurement of the ethylene and ethane permeability during the 4 bar H_2 stability test, as shown in Fig. S14. Utilizing Eq. (1) and Eq. (S9), the diffusivity and solubility of ethylene and ethane can be calculated for each point. As shown in Fig. 9(a) and Fig. 9(b), the diffusivity of ethylene increased slightly, while the solubility decreased—potentially caused by reduction of a small fraction of Ag^+ sites during H_2 permeation.

In summary, for both hydrogen stability experiments (i.e., 2 bar and 4 bar H_2 exposure), the ethylene-ethane permeability selectivity did not decrease within experimental uncertainty, even after 1152 h of H_2 exposure in the 2 bar experiment and 1779 h of H_2 exposure in the 4 bar experiment. Reduction of a small quantity of Ag^+ may have occurred, though a change in oxidation state of Ag^+ could not be detected by XPS for the 2 bar H_2 experiment (cf. Fig. 8(c)). For the 4 bar experiment, the slight increase in diffusivity and decrease in solubility for ethylene is consistent with reduction of a small quantity of Ag^+ to Ag^0. However, the observed effect is small, and the membranes maintain over 90% of the ethylene-ethane selectivity following long-term hydrogen exposure, a result not previously observed in polymeric facilitated transport membranes and substantially better than previously studied $AgBF_4$-PEBAX 2533 membranes.

Table 5
Calculation of the distance between Ag^+ cations in a 50 wt% $AgTf_2N$ XLPEGDA80 membrane based upon Eq. (4) and density measurements.

$AgTf_2N$ Concentration [wt. %]	Experimental Density [g cm^{-3}]	r_{Ag+} [Å]
0	1.159 ± 0.002	–
50	1.619 ± 0.002	9.3

3.5. *Effect of long-term ethylene permeation on ethylene permeability*

Multiple studies have found Ag^+ facilitated transport membranes to be unstable over long-term use, even without exposure to reducing gases [67]. Beyond the well-documented instability of Ag^+ facilitated transport membranes to H_2, olefin sorption in some Ag^+ facilitated transport membranes is not reversible. In a study of the $AgBF_4$-PEBAX 2533 polymer electrolytes discussed previously in the context of hydrogen stability, ethylene permeance decreased by an order of magnitude over the first few hours of ethylene permeation. Furthermore, successive equilibrium ethylene sorption isotherms showed incomplete desorption and decreased capacity [114]. As shown in Fig. 10(a), the $AgTf_2N$--containing XLPEGDA electrolytes showed only a 10% decrease in pure-gas ethylene permeability over 1392 h of ethylene permeation. In addition, the rate of decrease slowed significantly over the course of the experiment, implying that further ethylene permeation would have limited effect on ethylene permeability. Ethylene binding to Ag^+ sites in the $AgTf_2N$-XLPEGDA electrolytes was reversible, with sorption and desorption points falling on the same line indistinguishably, as seen in Fig. 10(b). In comparison to other studies of Ag^+ facilitated transport membranes, the $AgTf_2N$ XLPEGDA electrolytes show remarkable longevity and reversibility of ethylene binding.

4. Conclusions

A facile method of preparing stable polymeric Ag^+ facilitated transport membranes has been demonstrated. The pure-gas ethylene-ethane selectivity is much less sensitive to long-term H_2 exposure than other such membranes reported in literature, and no significant olefin conditioning was observed. Long-term H_2 stability studies were conducted at two different pressures of H_2, with the longest experiment lasting over ten weeks without a substantial decrease in ethylene-ethane selectivity. Further experiments are needed to confirm the mechanism of H_2 stability in the $AgTf_2N$ polymer electrolytes, but it is hypothesized to be the same steric protecting mechanism seen in Ag^+-containing ionic liquids. Further, overall performance of these membranes surpasses the ethylene-ethane upper bound, indicating favorable performance relative to previously explored polymeric gas separation membrane materials. High ethylene-ethane permeability selectivity in the $AgTf_2N$-containing membranes was found to result primarily from a large increase in solubility selectivity due to Ag^+ ions serving as preferential binding sites for olefins, also consistent with observed dual-mode sorption of ethylene. Facilitated transport of ethylene was found to shift ethylene-ethane diffusivity selectivity to less than one in the $AgTf_2N$-containing membrane—though ethylene is smaller than ethane. High olefin solubility in the $AgTf_2N$-containing membranes plasticizes the matrix and leads to increasing ethylene diffusivity and pure-gas ethylene-ethane selectivity with pressure. The results reported herein may begin to address a long-standing roadblock to reduction to practice in the field of Ag^+ facilitated transport membranes. Further studies are planned to characterize membrane properties key for industrial application, such as development of thin-film composite membranes with high permeance, membrane stability to H_2S and acetylene, membrane stability under mixed-gas conditions, the effect of plasticization by ethylene on mixed-gas transport properties, and the effect of temperature on Ag^+ stability and olefin-paraffin selectivity.

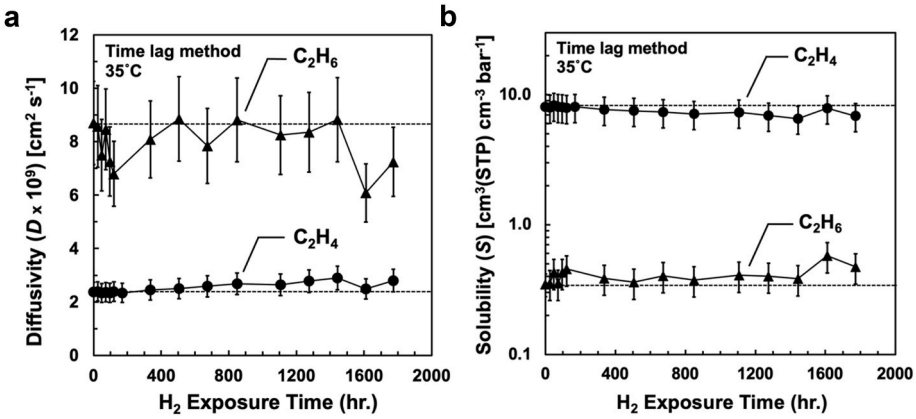

Fig. 9. (a) Diffusivity and (b) solubility of ethylene and ethane in a 50 wt% $AgTf_2N$ XLPEGDA80 membrane over the duration of permeation of 4 bar H_2 as calculated from time lag analysis. Error bars are calculated from propagating the uncertainty in the membrane thickness and the uncertainty of the time lag data shown in Fig. S14(a).

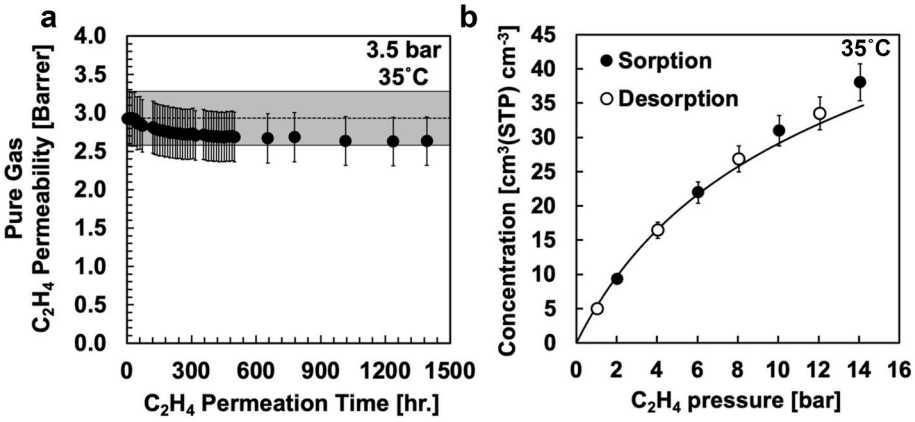

Fig. 10. (a) Pure-gas ethylene permeability as a function of pure-gas ethylene permeation time in a 50 wt% $AgTf_2N$ XLPEGDA80 membrane. The dotted line and grey band indicate the initial pure-gas C_2H_4/C_2H_6 selectivity and associated error prior to H_2 exposure. (b) Ethylene sorption isotherm with equilibrium measured at alternating pressure points for absorption and desorption. Error bars were calculated according to the same analysis as that in Fig. 4, and uptake was fitted with the previously discussed dual-mode sorption model (cf. Eq. (S6)).

Credit author statement

Matthew N. Davenport: Conceptualization, Methodology, Software, Validation, Formal analysis, Investigation, Resources, Data Curation, Writing – Original Draft, Writing – Review & Editing, Visualization, Project administration. **Caitlin L. Bentley:** Methodology, Validation, Formal analysis, Investigation, Data Curation, Writing – Review & Editing. **Joan F. Brennecke:** Conceptualization, Methodology, Validation, Resources, Writing – Review & Editing, Supervision, Project administration, Funding acquisition. **Benny D. Freeman:** Conceptualization, Methodology, Validation, Resources, Writing – Review & Editing, Supervision, Project administration, Funding acquisition.

Declaration of competing interest

The authors declare the following financial interests/personal relationships which may be considered as potential competing interests: M. N. Davenport, J. F. Brennecke, and B. D. Freeman are listed as inventors on a provisional patent application pending to The University of Texas System which covers the materials described in this article.

Acknowledgements

This article is based upon work supported in part by the National Science Foundation under Cooperative Agreement No. EEC-1647722. WAXS and XPS, GC-MS, ICP-OES, and density measurements were conducted in facilities operated in part by the Texas Materials Institute, the Mass Spectrometry Facility at the University of Texas at Austin (UT Austin), the UT Austin Environmental and Water Resources Engineering service center, and Professor Nate Lynd's research group at UT Austin, respectively. The authors gratefully acknowledge Dr. Oscar Morales-Collazo for synthesis of the $AgTf_2N$ salt, Dr. Hugo Celio for conducting the XPS measurements, James Burrow for fruitful discussions regarding analysis of WAXS and XPS data, and Rahul Sujanani and Alexander Bridge for preparing some of the membrane samples.

Appendix A. Supplementary information

Supplementary information for this article can be found online at https://doi.org/10.1016/j.memsci.2022.120300.

References

[1] A.H. Turner, Purity aspects of higher alpha olefins, JAOCS (J. Am. Oil Chem. Soc.) 60 (3) (1983) 623–627.
[2] W.R. True, Global ethylene capacity continues advance in 2011, Oil Gas J. 110 (7) (2012) 78–84.
[3] M. Bender, An overview of industrial processes for the production of olefins – C4 hydrocarbons, Chem. Bio. Eng. Rev. 1 (4) (2014) 136–147.
[4] S. Matar, L.F. Hatch, Crude Oil Processing and Production of Hydrocarbon Intermediates, Chemistry of Petrochemical Processes, Amsterdam, 2001, pp. 49–110.
[5] T. Ren, M. Patel, K. Blok, Olefins from conventional and heavy feedstocks: energy use in steam cracking and alternative processes, Energy 31 (4) (2006) 425–451.
[6] J.J.H.B. Sattler, J. Ruiz-Martinez, E. Santillan-Jimenez, B.M. Weckhuysen, Catalytic dehydrogenation of light alkanes on metals and metal oxides, Chem. Rev. 114 (20) (2014) 10613–10653.
[7] I. Amghizar, L.A. Vandewalle, K.M. Van Geem, G.B. Marin, New Trends in Olefin Production, Engineering 3, 2017, pp. 171–178 (2).

[8] Z. Zhao, J. Jiang, F. Wang, An economic analysis of twenty light olefin production pathways, J. Energy Chem. 56 (2021) 193–202.
[9] P. De Luna, C. Hahn, D. Higgins, S.A. Jaffer, T.F. Jaramillo, E.H. Sargent, What would it take for renewably powered electrosynthesis to displace petrochemical processes? Science 364 (6438) (2019) eaav3506.
[10] R.B. Eldridge, Olefin/paraffin separation technology: a review, Ind. Eng. Chem. Res. 32 (10) (1993) 2208–2212.
[11] V. Spallina, I.C. Velarde, J.A.M. Jimenez, H.R. Godini, F. Gallucci, M. Van Sint Annaland, Techno-economic assessment of different routes for olefins production through the oxidative coupling of methane (OCM): advances in benchmark technologies, Energy Convers. Manag. 154 (2017) 244–261.
[12] I. Nieuwoudt, N. Sanford, Overcoming challenges – Part Two, Hydrocarb. Eng. 12 (2019) 39–42.
[13] D.S. Sholl, R.P. Lively, Seven chemical separations to change the world, Nature 532 (7600) (2016) 435–437.
[14] A.I. Stankiewicz, J.A. Moulijn, Process intensification: transforming chemical engineering, Chem. Eng. Prog. 96 (2000) 22.
[15] National Academies of Sciences, Engineering, and Medicine, A Research Agenda for Transforming Separation Science, National Academies Press, Washington, DC, 2019.
[16] S. Pedram, T. Kaghazchi, M.T. Ravanchi, Performance and energy consumption of membrane-distillation hybrid systems for olefin-paraffin separation, Chem. Eng. Technol. 37 (4) (2014) 587–596.
[17] R. Zarca, A. Ortiz, D. Gorri, L.T. Biegler, I. Ortiz, Optimized distillation coupled with state-of-the-art membranes for propylene purification, J. Membr. Sci. 556 (2018) 321–328.
[18] T. Ridha, Y. Li, E. Gençer, J.J. Siirola, J.T. Miller, F.H. Ribeiro, R. Agrawal, Valorization of shale gas condensate to liquid hydrocarbons through catalytic dehydrogenation and oligomerization, Processes 6 (9) (2018) 1–21.
[19] M. Franklin, K. Chau, L.J. Cushing, J.E. Johnston, Characterizing flaring from unconventional oil and gas operations in South Texas using satellite observations, Environ. Sci. Technol. 53 (4) (2019) 2220–2228.
[20] A. Motelica, O.S.L. Bruinsma, R. Kreiter, M. den Exter, J.F. Vente, Membrane retrofit option for paraffin/olefin separation—a technoeconomic evaluation, Ind. Eng. Chem. Res. 51 (19) (2012) 6977–6986.
[21] J.G. Wijmans, R.W. Baker, The solution-diffusion model: a review, J. Membr. Sci. 107 (1) (1995) 1–21.
[22] K. Ghosal, B.D. Freeman, Gas separation using polymer membranes: an overview, Polym. Adv. Technol. 5 (11) (1994) 673–697.
[23] R.L. Burns, W.J. Koros, Defining the challenges for C3H6/C3H8 separation using polymeric membranes, J. Membr. Sci. 2 (211) (2003) 299–309.
[24] C. Staudt-Bickel, W.J. Koros, Olefin/paraffin gas separations with 6FDA-based polyimide membranes, J. Membr. Sci. 170 (2) (2000) 205–214.
[25] L.M. Robeson, Correlation of separation factor versus permeability for polymeric membranes, J. Membr. Sci. 62 (2) (1991) 165–185.
[26] M. Rungta, C. Zhang, W.J. Koros, L. Xu, Membrane-based ethylene/ethane separation: the upper bound and beyond, AIChE J. 59 (9) (2013) 3475–3489.
[27] R.C. Reid, J.M. Prausnitz, B.E. Poling, The Properties of Gases and Liquids, 1987.
[28] J.-R. Li, R.J. Kuppler, H.-C. Zhou, Selective gas adsorption and separation in metal–organic frameworks, Chem. Soc. Rev. 38 (5) (2009) 1477–1504.
[29] K. Tanaka, A. Taguchi, J. Hao, H. Kita, K. Okamoto, Permeation and separation properties of polyimide membranes to olefins and paraffins, J. Membr. Sci. 121 (2) (1996) 197–207.
[30] Y. Li, S. Wang, G. He, H. Wu, F. Pan, Z. Jiang, Facilitated transport of small molecules and ions for energy-efficient membranes, Chem. Soc. Rev. 44 (1) (2015) 103–118.
[31] C.K. Kim, K.A. Lee, C.K. Kim, B.S. Lee, H.W. Lee, NBO analyses of the back-bonding in metal-olefin complexes, Chem. Phys. Lett. 391 (4–6) (2004) 321–324.
[32] Y.S. Kang, J.O. Won, B.S. Jung, H.H. Park, S.G. Oh, Solid state polymer electrolyte facilitated transport membranes containing surfactants, Korea Adv. Instit. Sci. Technol. U.S 6 (2003) 276, 645.
[33] T. Yamaguchi, C. Baertsch, C.A. Koval, R.D. Noble, C.N. Bowman, Olefin separation using silver impregnated ion-exchange membranes and silver salt/polymer blend membranes, J. Membr. Sci. 117 (1–2) (1996) 151–161.
[34] M.R. Antonio, D.T. Tsou, Silver ion coordination in membranes for facilitated olefin transport, Ind. Eng. Chem. Res. 32 (2) (1993) 273–278.
[35] D.J. Safarik, R.B. Eldridge, Olefin/paraffin separations by reactive absorption: a review, Ind. Eng. Chem. Res. 37 (7) (1998) 2571–2581.
[36] A. Ortiz, L.M. Galán Sanchez, D. Gorri, A.B. De Haan, I. Ortiz, Reactive ionic liquid media for the separation of propylene/propane gaseous mixtures, Ind. Eng. Chem. Res. 49 (16) (2010) 7227–7233.
[37] F. Agel, F. Pitsch, F.F. Krull, P. Schulz, M. Wessling, T. Melin, P. Wasserscheid, Ionic liquid silver salt complexes for propene/propane separation, Phys. Chem. Chem. Phys. 13 (2) (2011) 725–731.
[38] C.M. Sanchez, T. Song, J.F. Brennecke, B.D. Freeman, Hydrogen stable supported ionic liquid membranes with silver carriers: propylene and propane permeability and solubility, Ind. Eng. Chem. Res. 59 (2019) 5362–5370.
[39] S. Park, O. Morales-Collazo, B.D. Freeman, J.F. Brennecke, Ionic Liquid Stabilizes Olefin Facilitated Transport Membranes against Reduction, (unpublished work).
[40] S.Y. Kim, Y. Cho, S.W. Kang, Preparation and characterization of PEBAX-5513/AgBF4/BMIMBF4 membranes for olefin/paraffin separation, Polymers 12 (7) (2020) 1550.
[41] S.W. Kang, K. Char, J.H. Kim, C.K. Kim, Y.S. Kang, Control of ionic interactions in silver Salt−Polymer complexes with ionic liquids: implications for facilitated olefin transport, Chem. Mater. 18 (7) (2006) 1789–1794.
[42] H. Dou, B. Jiang, X. Xiao, M. Xu, B. Wang, L. Hao, Y. Sun, L. Zhang, Ultra-stable and cost-efficient protic ionic liquid based facilitated transport membranes for highly selective olefin/paraffin separation, J. Membr. Sci. 557 (2018) 76–86.
[43] T.C. Merkel, Z. He, A. Morisato, I. Pinnau, Olefin/paraffin solubility in a solid polymer electrolyte membrane, Chem. Commun. 13 (April) (2003) 1596–1597.
[44] Y. Yoon, J. Won, Y.S. Kang, Polymer electrolyte membranes containing silver ion for facilitated olefin transport, Macromolecules 33 (9) (2000) 3185–3186.
[45] I. Pinnau, L.G. Toy, Solid polymer electrolyte composite membranes for olefin/paraffin separation, J. Membr. Sci. 184 (1) (2001) 39–48.
[46] S. Sunderrajan, Propane and propylene sorption in solid polymer electrolytes based on poly(ethylene oxide) and silver salts, J. Membr. Sci. 182 (1–2) (2001) 1–12.
[47] J.H. Kim, B.R. Min, J. Won, Y.S. Kang, Complexation mechanism of olefin with silver ions dissolved in a polymer matrix and its effect on facilitated olefin transport, Chem. Eur J. 8 (3) (2002) 650–654.
[48] S.U. Hong, C.K. Kim, Y.S. Kang, Measurement and analysis of propylene solubility in polymer electrolytes containing silver salts, Macromolecules 33 (21) (2000) 7918–7921.
[49] A. Morisato, Z. He, I. Pinnau, T.C. Merkel, Transport properties of PA 12-PTMO/AgBF4 solid polymer electrolyte membranes for olefin/paraffin separation, Desalination 145 (2002) 347–351.
[50] Y. Wang, J. Ren, M. Deng, Ultrathin solid polymer electrolyte PEI/Pebax2533/AgBF4 composite membrane for propylene/propane separation, Separ. Purif. Technol. 77 (1) (2011) 46–52.
[51] J.H. Kim, J. Won, Y.S. Kang, π-complexes of polystyrene with silver salts and their use as facilitated olefin transport membranes, J. Polym. Sci. B Polym. Phys. 42 (12) (2004) 2263–2269.
[52] R.G. Pearson, Hard and soft acids and bases, HSAB, part 1: fundamental principles, J. Chem. Educ. 45 (9) (1968) 581.
[53] F.M. Gray, Solid Polymer Electrolytes, VCH Publishers, Hoboken, NJ, USA, 1991.
[54] R. Faiz, K. Li, Olefin/paraffin separation using membrane based facilitated transport/chemical absorption techniques, Chem. Eng. Sci. 73 (2012) 261–284.
[55] S. Sunderrajan, Facilitated Transport of Gases through Polymeric Membranes : Experiment and Computer Simulations, North Carolina State University, 1996.
[56] Y.S. Kang, J.M. Hong, J. Jang, U.Y. Kim, Analysis of facilitated transport in solid membranes with fixed site carriers: 1. Single RC circuit model, J. Membr. Sci. 109 (2) (1996) 149–157.
[57] C.K. Kim, C.K. Kim, B.-S. Lee, J. Won, H.S. Kim, Y.S. Rang, Density functional theory studies on the reaction mechanisms of silver ions with ethylene in facilitated transport membranes: a modeling study, J. Phys. Chem. 105 (39) (2001) 9024–9028.
[58] R. Zarca, A. Ortiz, D. Gorri, I. Ortiz, Generalized predictive modeling for facilitated transport membranes accounting for fixed and mobile carriers, J. Membr. Sci. 542 (August) (2017) 168–176.
[59] P. Meares, The diffusion of gases through polyvinyl acetate, J. Am. Chem. Soc. 76 (13) (1954) 3415–3422.
[60] A.Y. Alentiev, Y.P. Yampolskii, Meares equation and the role of cohesion energy density in diffusion in polymers, J. Membr. Sci. 206 (1–2) (2002) 291–306.
[61] J.H. Kim, B.R. Min, C.K. Kim, J. Won, Y.S. Kang, Spectroscopic interpretation of silver ion complexation with propylene in silver polymer electrolytes, J. Phys. Chem. B 106 (10) (2002) 2786–2790.
[62] Y.M. Chen, J.L. Elkind, P.B. Armentrout, Reactions of Ru+, Rh+, Pd+, and Ag+ with H2, HD, and D2, J. Phys. Chem. 99 (26) (1995) 10438–10445.
[63] A. Takahashi, R.T. Yang, C.L. Munson, D. Chinn, Influence of Ag content and H2S exposure on 1,3-butadiene/1-butene adsorption by Ag ion-exchanged Y-Zeolites (Ag−Y), Ind. Eng. Chem. Res. 40 (18) (2001) 3979–3988.
[64] T.C. Merkel, R. Blanc, I. Ciobanu, B. Firat, A. Suwarlim, J. Zeid, Silver salt facilitated transport membranes for olefin/paraffin separations: carrier instability and a novel regeneration method, J. Membr. Sci. 447 (2013) 177–189.
[65] D.-Y. Lee, A. Elgowainy, By-product hydrogen from steam cracking of natural gas liquids (NGLs): potential for large-scale hydrogen fuel production, life-cycle air emissions reduction, and economic benefit, Int. J. Hydrogen Energy 43 (43) (2018) 20143–20160.
[66] J.G. Speight, Handbook of Petrochemical Processes, 2019. Boca Raton, FL.
[67] A.C.C. Campos, R.A. Dos Reis, A. Ortiz, D. Gorri, I. Ortiz, A perspective of solutions for membrane instabilities in olefin/paraffin separations: a review, Ind. Eng. Chem. Res. 57 (31) (2018) 10071–10085.
[68] S.W. Kang, K. Char, J.H. Kim, Y.S. Kang, Ionic liquid as a solvent and the long-term separation performance in a polymer/silver salt complex membrane, Macromol. Res. 15 (2) (2007) 167–172.
[69] S.W. Kang, J.H. Kim, J. Won, Y.S. Kang, Suppression of silver ion reduction by Al(NO3)3 complex and its application to highly stabilized olefin transport membranes, J. Membr. Sci. 445 (2013) 156–159.
[70] Y. Sung Park, Y. Soo Kang, S. Wook Kang, Cost-effective facilitated olefin transport membranes consisting of polymer/AgCF3SO3/Al(NO3)3 with long-term stability, J. Membr. Sci. 495 (2015) 61–64.
[71] P. Eor, D. Ryoo, H. Nan, J.L. Anderson, Characterizing olefin selectivity and stability of silver salts in ionic liquids using inverse gas chromatography, ACS Omega 5 (48) (2020) 31362–31369.
[72] R.B. Baird, A.D. Eaton, E.W. Rice, Standard Methods for the Examination of Water and Wastewater, 23rd ed., 2017. Washington, D.C.
[73] H. Lin, T. Kai, B.D. Freeman, S. Kalakkunnath, D.S. Kalika, The effect of cross-linking on gas permeability in cross-linked poly(ethylene glycol diacrylate), Macromolecules 38 (20) (2005) 8381–8393.
[74] D.J. Waters, K. Engberg, R. Parke-Houben, L. Hartmann, C.N. Ta, M.F. Toney, C. W. Frank, Morphology of photopolymerized end-linked poly(ethylene glycol)

hydrogels by small-angle X-ray scattering, Macromolecules 43 (16) (2010) 6861–6870.
[75] P. Malo de Molina, S. Lad, M.E. Helgeson, Heterogeneity and its influence on the properties of difunctional poly(ethylene glycol) hydrogels: structure and mechanics, Macromolecules 48 (15) (2015) 5402–5411.
[76] H. Lin, B.D. Freeman, Permeation and diffusion, in: H. Czichos, T. Saito, L. R. Smith (Eds.), Handbook of Materials Measurement Methods, Springer, New York, NY, USA, 2006, pp. 371–387.
[77] T. Song, O. Morales-Collazo, J.F. Brennecke, Solubility and diffusivity of oxygen in ionic liquids, J. Chem. Eng. Data 64 (11) (2019) 4956–4967.
[78] T. Song, M.J. Lubben, J.F. Brennecke, Solubility of argon, krypton and xenon in ionic liquids, Fluid Phase Equil. 504 (2020) 112334.
[79] H. Lin, E. Wagner, J. Swinnea, B. Freeman, S. Pas, A. Hill, S. Kalakkunnath, D. Kalika, Transport and structural characteristics of crosslinked poly(ethylene oxide) rubbers, J. Membr. Sci. 276 (1–2) (2006) 145–161.
[80] M. Repoux, Comparison of background removal methods for XPS, Surf. Interface Anal. 18 (7) (1992) 567–570.
[81] Y.M. Mohan, T. Premkumar, K. Lee, K.E. Geckeler, Fabrication of silver nanoparticles in hydrogel networks, Macromol. Rapid Commun. 27 (16) (2006) 1346–1354.
[82] I. Coblentz Society, Evaluated infrared reference spectra, in: P.J. Linstrom, W.G. Mallard (Eds.), NIST Chemistry WebBook, National Institute of Standards and Technology, Gaithersburg, MD.
[83] P. Raut, S. Li, Y.-M. Chen, Y. Zhu, S.C. Jana, Strong and flexible composite solid polymer electrolyte membranes for Li-ion batteries, ACS Omega 4 (19) (2019) 18203–18209.
[84] H.A. Albehaijan, C.R. Piedrahita, J. Cao, M. Soliman, S. Mitra, T. Kyu, Mechanoelectrical transduction of polymer electrolyte membranes: effect of branched networks, ACS Appl. Mater. Interfaces 12 (6) (2020) 7518–7528.
[85] J.-F.L. Nest, A. Gandini, H. Cheradame, Crosslinked polyethers as media for ionic conduction, Br. Polym. J. 20 (3) (1988) 253–268.
[86] S. Lascaud, M. Perrier, A. Vallee, S. Besner, J. Prud'homme, M. Armand, Phase diagrams and conductivity behavior of poly(ethylene oxide)-molten salt rubbery electrolytes, Macromolecules 27 (25) (1994) 7469–7477.
[87] N.A. Stolwijk, C. Heddier, M. Reschke, M. Wiencierz, J. Bokeloh, G. Wilde, Salt-concentration dependence of the glass transition temperature in PEO–NaI and PEO–LiTFSI polymer electrolytes, Macromolecules 46 (21) (2013) 8580–8588.
[88] M. Rungta, L. Xu, W.J. Koros, Carbon molecular sieve dense film membranes derived from Matrimid® for ethylene/ethane separation, Carbon 50 (4) (2012) 1488–1502.
[89] J. Ploegmakers, S. Japip, K. Nijmeijer, Mixed matrix membranes containing MOFs for ethylene/ethane separation Part A: membrane preparation and characterization, J. Membr. Sci. 428 (2013) 445–453.
[90] L.C. Tomé, D. Mecerreyes, C.S.R. Freire, L.P.N. Rebelo, I.M. Marrucho, Polymeric ionic liquid membranes containing IL–Ag+ for ethylene/ethane separation via olefin-facilitated transport, J. Mater. Chem. 2 (16) (2014) 5631.
[91] J.E. Bachman, Z.P. Smith, T. Li, T. Xu, J.R. Long, Enhanced ethylene separation and plasticization resistance in polymer membranes incorporating metal–organic framework nanocrystals, Nat. Mater. 15 (8) (2016) 845–849.
[92] O. Salinas, X. Ma, E. Litwiller, I. Pinnau, Ethylene/ethane permeation, diffusion and gas sorption properties of carbon molecular sieve membranes derived from the prototype ladder polymer of intrinsic microporosity (PIM-1), J. Membr. Sci. 504 (2016) 133–140.
[93] O. Salinas, X. Ma, Y. Wang, Y. Han, I. Pinnau, Carbon molecular sieve membrane from a microporous spirobisindane-based polyimide precursor with enhanced ethylene/ethane mixed-gas selectivity, RSC Adv. 7 (6) (2017) 3265–3272.
[94] Y.-H. Chu, D. Yancey, L. Xu, M. Martinez, M. Brayden, W. Koros, Iron-containing carbon molecular sieve membranes for advanced olefin/paraffin separations, J. Membr. Sci. 548 (2018) 609–620.
[95] H. Dou, B. Jiang, M. Xu, J. Zhou, Y. Sun, L. Zhang, Supported ionic liquid membranes with high carrier efficiency via strong hydrogen-bond basicity for the sustainable and effective olefin/paraffin separation, Chem. Eng. Sci. 193 (2019) 27–37.
[96] H.L. Clever, Setchenov salt-effect parameter, J. Chem. Eng. Data 28 (3) (1983) 340–343.
[97] E. Ruckenstein, I. Shulgin, Salting-out or -in by fluctuation theory, Ind. Eng. Chem. Res. 41 (18) (2002) 4674–4680.
[98] J.H. Kim, S.M. Park, J. Won, Y.S. Kang, Unusual separation property of propylene/propane mixtures through polymer/silver complex membranes containing mixed salts, J. Membr. Sci. 248 (1–2) (2005) 171–176.
[99] W. Hayduk, Solubility Data Series - Ethane, Pergamon Press, Oxford, 1982.
[100] O.M. Ilinitch, G.L. Semin, M.V. Chertova, K.I. Zamaraev, Novel polymeric membranes for separation of hydrocarbons, J. Membr. Sci. 66 (1) (1992) 1–8.
[101] D.G. Shaw, P. Scharlin, R.P.T. Tomkins, E. Wilhelm, Y.P. Yampol'skii, P.O. Gujral, Solubility Data Series - Ethene, Oxford University Press, Oxford, 1994.
[102] E.S. Zofchak, Z. Zhang, B. Wheatle, R. Sujanani, S.J. Warnock, T. J. Dilenschneider, K.G. Hanson, S. Zhao, S. Mukherjee, M.M. Abu-Omar, C. M. Bates, B.D. Freeman, V. Ganesan, Origins of lithium/sodium reverse permeability selectivity in 12-crown-4-functionalized polymer membranes, ACS Macro Lett. (2021) in press.
[103] S.J. Warnock, R. Sujanani, E.S. Zofchak, S. Zhao, T.J. Dilenschneider, K. G. Hanson, S. Mukherjee, V. Ganesan, B.D. Freeman, M.M. Abu-Omar, C.M. Bates, Selective lithium transport with 12-Crown-4-functionalized polynorbornene membranes, Proc. Natl. Acad. Sci. Unit. States Am. 118 (2021) in press.
[104] J. Won, Y. Yoon, Y.S. Kang, Changes in facilitated transport behavior of silver polymer electrolytes by UV irradiation, Macromol. Res. 10 (2) (2002) 80–84.
[105] V.K. Kaushik, XPS core level spectra and Auger parameters for some silver compounds, J. Electron. Spectrosc. Relat. Phenom. 56 (3) (1991) 273–277.
[106] P. He, H. Liu, Z. Li, Y. Liu, X. Xu, J. Li, Electrochemical deposition of silver in room-temperature ionic liquids and its surface-enhanced Raman scattering effect, Langmuir 20 (23) (2004) 10260–10267.
[107] A. Basile, A.I. Bhatt, A.P. O'Mullane, S.K. Bhargava, An investigation of silver electrodeposition from ionic liquids: influence of atmospheric water uptake on the silver electrodeposition mechanism and film morphology, Electrochim. Acta 56 (7) (2011) 2895–2905.
[108] T. Liu, Electrodéposition de couches minces métalliques à partir de solutions de liquides ioniques pour des applications électroniques, University of Bordeaux, 2014.
[109] Z.H. Liu, Y. Li, K.W. Kowk, Mean interparticle distances between hard particles in one to three dimensions, Polymer 42 (6) (2001) 2701–2706.
[110] R.D. Shannon, Revised effective ionic radii and systematic studies of interatomic distances in halides and chalcogenides, Acta Crystallogr. A 32 (5) (1976) 751–767.
[111] S. Perkin, L. Crowhurst, H. Niedermeyer, T. Welton, A.M. Smith, N.N. Gosvami, Self-assembly in the electrical double layer of ionic liquids, Chem. Commun. 47 (23) (2011) 6572–6574.
[112] H.-W. Cheng, P. Stock, B. Moeremans, T. Baimpos, X. Banquy, F.U. Renner, M. Valtiner, Characterizing the influence of water on charging and layering at electrified ionic-liquid/solid interfaces, Adv. Mater. Interfac. 2 (12) (2015) 1500159.
[113] J.B. Haskins, W.R. Bennett, J.J. Wu, D.M. Hernández, O. Borodin, J.D. Monk, C. W. Bauschlicher, J.W. Lawson, Computational and experimental investigation of Li-doped ionic liquid electrolytes: [pyr14][TFSI], [pyr13][FSI], and [EMIM][BF4], J. Phys. Chem. B 118 (38) (2014) 11295–11309.
[114] T.C. Merkel, R. Blanc, J. Zeid, A. Suwarlim, B. Firat, H. Wijmans, M. Asaro, M. Greene, Separation of Olefin/Paraffin Mixtures with Carrier Facilitated Membranes, U.S. Department of Energy, 2007.